Fuel 292 (2021) 120296

EXPERIMENTAL ANALYSIS OF THE INJECTION PRESSURE EFFECT ON THE NEAR-FIELD STRUCTURE OF LIQUID FUEL SPRAYS

Salvador, F.J. (*), Gimeno, J., De la Morena, J., González-Montero, L.A.

CMT-Motores Térmicos, Universitat Politècnica de València

Camino de Vera s/n, E-46022, Valencia, Spain.

(*) Corresponding author:

Dr. F. Javier Salvador, fsalvado@mot.upv.es

CMT-Motores Térmicos, Universitat Politècnica de València

Camino de Vera s/n, E-46022, Valencia, Spain.

Telephone: +34-963879659

FAX: +34-963877659

Keywords

spray, turbulence, atomization, mixing, visualization

Abstract

Primary atomization and initial spray development are critical in the operation of high-pressure liquid sprays such as the ones used in internal combustion engines. In the current paper, an analysis of the effect of the fuel injection pressure on the near-nozzle spray morphology is performed. For this purpose, a high-magnification diffused backlight

imaging technique is set by means of a high-speed light-emitting diode and a long-distance microscope. The technique allows to visualize the first 2 millimeters of the spray development with a resolution of approximately 250 pixels per millimeter. The images obtained are processed with two different criteria to define the spray contour: one using an optical thickness threshold and a second one based on the intensity derivative on the radial direction. The analysis is focused on three aspects of the spray morphology: the spray angle, its standard deviation, and the standard deviation of the spray contour itself. The results show that the average spray angle is only slightly affected by the injection pressure, being the discharge density the main boundary condition affecting this parameter. Instead, the two standard deviation parameters show a clear increasing trend with the injection pressure, confirming that higher turbulence at the nozzle outlet induces higher variability in the spray shape. Regarding the two contour detection methodologies, similar values are reached in the average spray angle, while some more impact is seen in the spray dispersion, although the same trends are found.

NOMENCLATURE

CMOS	Complementary metal-oxide semiconductor sensor
DBI	Diffused backlight illumination
GDI	Gasoline direct-injection
I	Intensity acquired by the CMOS sensor
I_0	Intensity of the background light
KL	Optical thickness
LED	Light-emitting diode
P_{inj}	Fuel injection pressure

P_{back}	Discharge pressure
x	Axial direction in spray images
y	Radial direction in spray images

Greek Symbols

ρ	Density of the fluid
μ	Dynamic viscosity of the fluid
σ	Standard deviation of the spray contour

1. Introduction

Liquid sprays are used in a variety of applications, from manufacturing processes to pharmaceutical industry or propulsion applications. In the particular case of direct-injection engines, the fuel injection process critically affects the subsequent combustion development and emissions formation. For gasoline direct-injection (GDI) engines, Oh and Bae [1] showed how the fuel injection timing impacts mixture stratification, leading to significant differences in soot and unburned hydrocarbons emissions. Roque et al. [2] studied the interaction between the GDI spray and the piston surface as one of the main root causes for soot formation. In compression-ignition engines, the impact of the spray formation on the combustion evolution is even clearer. On the one hand, spray features affect the flame structure in terms of lift-off length [3,4], soot formation and oxidation [5,6], temperature distribution [7] and the interaction with the combustion chamber walls [8,9]. On the other hand, these processes control the heat release rate characteristics [10,11] and the exhaust emissions at the engine-out [12,13], which can be particularly critical in cold-start conditions [14].

Primary atomization is one of the most critical aspects involved in the development of liquid sprays [15]. However, it is a complex process produced as a result of multiple phenomena. First, primary atomization is affected by the particular features of the internal nozzle flow [16,17], especially when cavitation occurs, since the collapse of the cavitation could can induce a distortion of the liquid spray boundary [18,19]. Surface tension [20] and aerodynamic forces [21,22] are also key mechanisms in the initial break-up of the liquid core. In the same sense, the interaction between the spray and the flow characteristics in the discharge chamber also plays a role [23]. Finally, turbulence induced vortices in the liquid spray surface promote the formation of ligaments and droplets [24,25], leading to a complete atomization regimes for high velocity sprays such as the ones typical of compression-ignition engines.

Several experimental methodologies have been developed to analyze primary atomization and its impact on spray formation by means of optical diagnostics. Kim and Park [26] used backlight illumination to evaluate the effect of the nozzle geometry on cavitation formation and initial spray opening in two-dimensional large scale nozzles. Linne et al. [27] developed the ballistic imaging technique as a means to observe the spray structure in the near-nozzle dense spray region. Payri et al. [28] developed a high-magnification imaging using a Yag-Nd laser and evaluated the amplitude and wavelength of the oscillations inside the spray contour. Duke et al. [29] used x-ray tomography to analyze the projected mass distribution inside this initial portion of the spray. Payri et al. [30] analyzed the initial spray angle and its variability through high-speed and high-magnification diffused backlight illumination (DBI), achieved by means of a light-emitting diode (LED) and a long distance microscope lens. Manin et al [31] used a similar arrangement to evaluate the effects of fuel properties on the near-field spray characteristics, comparing n-dodecane and ethanol.

In the current paper, a detailed analysis of the influence of the fuel injection pressure on the characteristics of the spray in the near-nozzle region has been performed. The aim of this study is to shed light on the relationship between the turbulence induced by this injection pressure (linked to high spray outlet velocity) and the spray opening angle as well as the standard deviation of the spray contour, which is a marker for the oscillations in the spray boundary. This analysis is performed in quasi-stationary conditions, when the injector needle is far from its seat, so that the spray is not influenced by the details of the needle geometry and dynamics. For this purpose, high-magnification DBI visualization achieved by means of a long-distance microscope is used on a constant-volume chamber pressurized with nitrogen at room temperature (i.e. inert non-evaporative conditions). The test plan includes 5 levels of injection pressure (from 50 to 150 MPa) and two levels of discharge pressure (1 and 4 MPa) for a single-hole axi-symmetric nozzle. The images are post-processed using two different criteria for detecting the spray boundary: one based on a threshold of the optical thickness, and a second one considering the derivative of the image intensity.

As far as the paper structure is concerned, Section 2 reviews the experimental setup and conditions used for the analysis. The main features of the image postprocessing are described in Section 3. Section 4 depicts and discuss the main results and findings obtained along the study. Finally, the main conclusions are summarized in Section 5.

2. Experimental setup

Figure 1 shows a schematic view of the experimental arrangement used for the visualization campaign. A diffused backlight illumination (DBI) technique is configured. For this purpose, a constant volume chamber with two opposite windows is selected. Illumination is provided through a high-speed light-emitting diode (LED), characterized

by a pulse duration of 70 ns. On the other side, a high speed Photron Fastcam SA-Z CMOS camera is coupled to a long-distance K2 DistaMax microscope with a CF-2 objective to achieve a large magnification of the spray in the near-nozzle field. The camera acquires 175000 frames per second with an imaging window of 512x168 pixels, allowing to visualize approximately the first 2 millimeters of the spray with a resolution of approximately 247 pixels per millimeter.

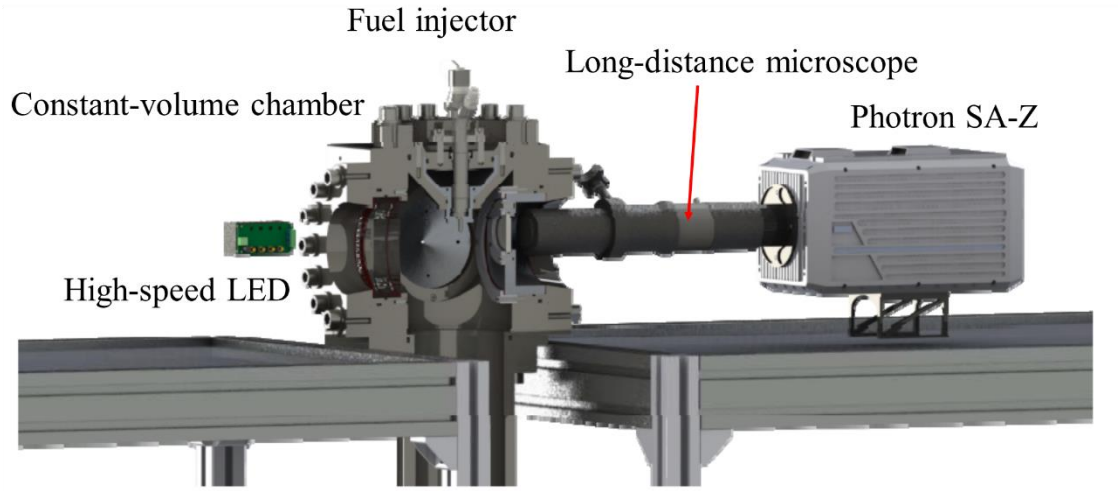

Figure 1: Diffused backlight visualization setup

Using this arrangement, a total of 10 operating conditions were evaluated, including 5 levels of injection pressure (50, 80, 100, 120 and 150 MPa) and two levels of discharge pressure (1 and 4 MPa), leading to ambient densities of 11.3 and 45.4 kg/m^3, respectively. Each test was repeated 10 times in order to ensure the consistency of the results. All tests were achieved with a piezoeletric-driven diesel fuel injector, equipped with a single-hole axi-symmetric nozzle, including a nozzle nominal outlet diameter of 0.090 mm and a high degree of conicity, so that cavitation formation inside the nozzle orifice can be avoided. Using this kind of configuration instead of a multi-hole nozzle, traditionally appearing in diesel engines, allowed to use single-pass DBI configuration and avoid spray-to-spray interactions, increasing the fidelity of the results produced. The injector ran with n-

dodecane fuel, whose main physical properties are gathered on Table 1 for the experimental conditions used along the tests. These values have been obtained using similar expressions as the ones found in [32] as a function of pressure, but adapted for n-dodecane based on the information in [33]. A constant duration of the electronic pulse to the piezoeletric valve of 2 ms is selected to ensure that the hydraulic duration of the injection event is long enough. A sample of the images obtained are presented in Figure 2 where two different frames corresponding to the same injection pressure (150 MPa) but at different discharge pressure (1 and 4 MPa).

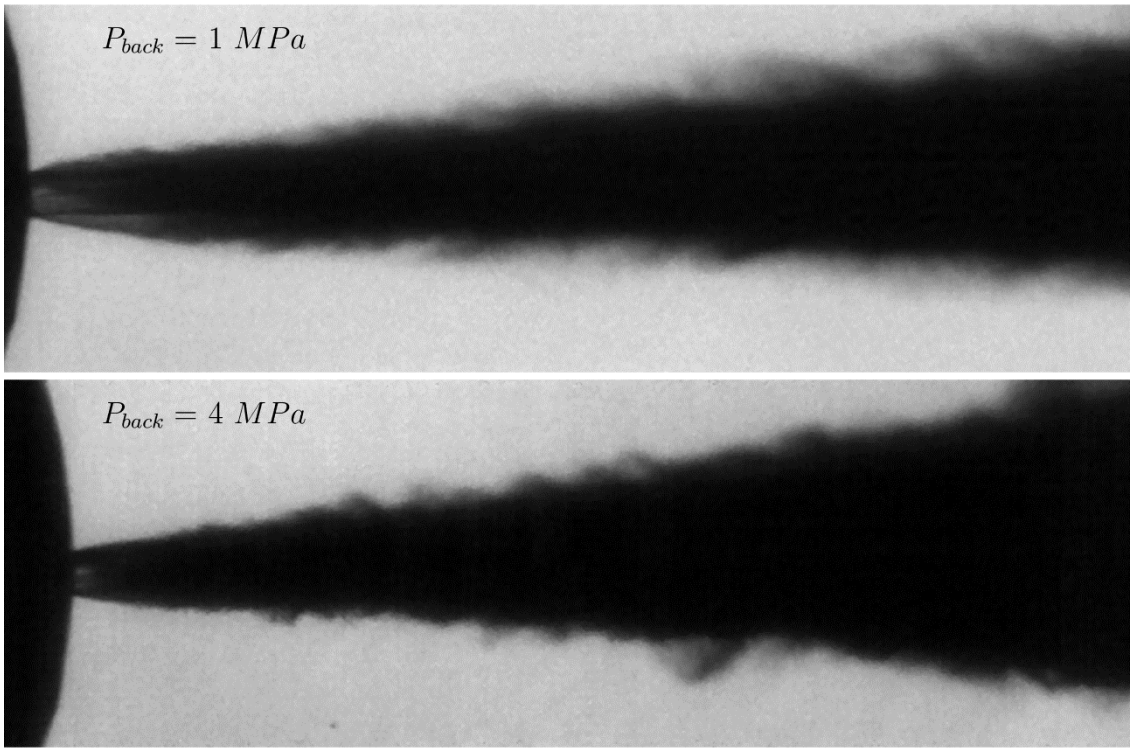

Figure 2: Instantaneous frames of two injection events with P_{inj}=150 MPa and P_{back}=1 MPa (top) and P_{back}= 4 MPa (bottom)

Table 1: fuel (n-dodecane) density and viscosity as a function of pressure

P_{inj} [MPa]	50	80	100	120	150
ρ [kg/m^3]	774.90	789.26	797.74	805.52	816.14
μ [mPa·s]	2.24	2.96	3.54	4.21	5.41

3. Spray contour detection

The analysis performed in the current work focuses on the analysis of the near-nozzle spray contour in quasi-stationary conditions, once the needle is at a high-enough position not to affect the spray development. Therefore, only the images corresponding to this part of the injection event are considered.

Due to the high level of magnification achieved in the current setup, the images are subjected to slight variability in their position induced by vibrations either in the camera or in the injector itself. These variations are corrected by a proper alignment of the nozzle tip boundary between experiments. From that point on, the center of the coordinate system is placed at the furthest position of this nozzle tip contour.

Two methodologies are evaluated in order to determine the spray contour on each image. The first one is based in the Beer-Lambert-Bouguer law which relates the attenuation of the light travelling through a material and is expressed as Eq. (1) and has been already used in previous spray DBI research works [34].

$$KL = -ln\left(\frac{I}{I_0}\right) \tag{1}$$

Where KL is the optical thickness, I is the light intensity registered by the CMOS sensor in each frame and I_0 is the background luminosity obtained in each repetition by averaging the frames previous to the start of the injection. However, this methodology may be sensitive to slight variations in the intensity levels produced by variabilities in the light source operation or reduction in the windows' cleanliness. Therefore, a second methodology is proposed using as a measuring factor not the absolute intensity level, but the intensity derivative along the cross direction after a signal treatment to reduce the

noise on the intensity profile. The main advantage is that the location of the maximum peaks of this parameter can be located automatically, so no calibration is needed.

Figure 3 shows an example of both methodologies for an axial distance of 1.15 mm from the nozzle exit and for the operation condition of 150 MPa injection pressure and 1 MPa discharge pressure, being the KL based method represented in black and the intensity derivative depicted in grey. Focusing on KL method, it can be observed that when there is no interaction between the LED and the spray KL values around zero are obtained. Once the spray droplets deviate the incident light, the KL rapidly increases until reaching a maximum value at the spray center. Therefore, it is usual to define a threshold of this parameter to distinguish the spray contour from the background. Due to the KL variations at the spray region, an average of the KL is done on the maximum flat area to get an approximation of its maximum value for each axial distance and frame. In the current work, after a preliminary evaluation, the threshold is set to the 5% of the averaged value of the maximum KL obtained at each axial position. On the contrary, the intensity derivative (grey curve) shows two peaks with a narrow width (around 50 μm width) that correspond with the maximum intensity variation from background light to spray

absorption for both sides. Therefore, the locations of these minimum and maximum intensity derivative values at each axial position can be used to detect the spray boundary.

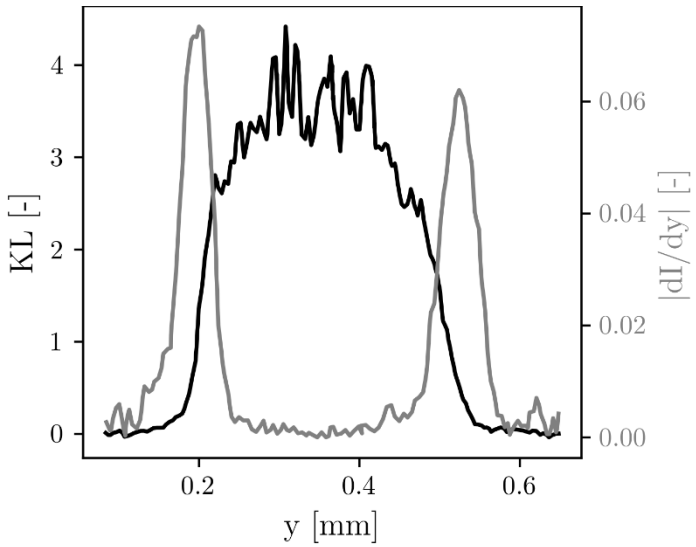

Figure 3: Contour detection method comparison on lateral profile. P_{inj}=150 MPa; P_{back}= 1 MPa; x= 1.15 mm. Black KL method, Grey derivative method

Finally, both criteria are applied to each axial position to detect the whole spray contour. Figure 4 shows the result of applying the two methodologies previously explained to a specific image from the same experimental condition. In the figure, the green line represents the detected contour using the threshold applied to the KL, while the yellow line shows the outcome when the intensity derivative criterion is selected. As it can be seen, both criteria produce very similar results, while the intensity derivative one seems to be slightly more sensitive and produce spray contours with higher fluctuations.

However, the impact of the imaging processing technique on the results will be discussed in the next section.

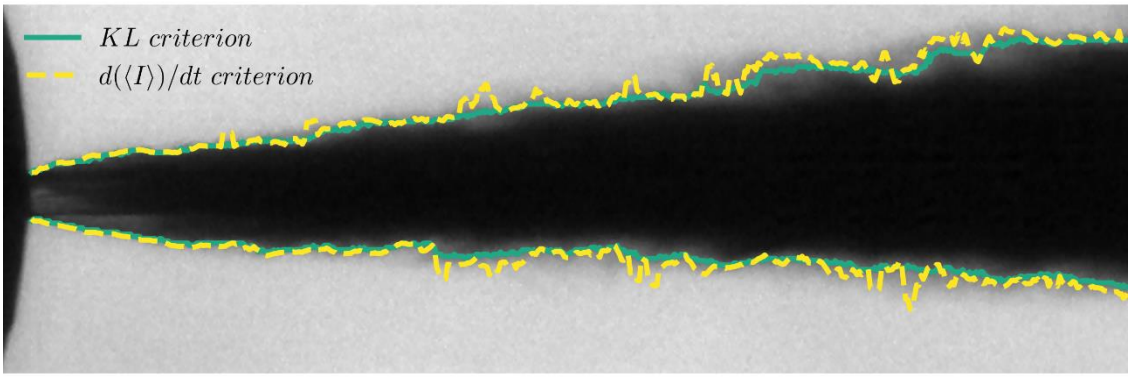

Figure 4: Example of image processing result. P_{inj}=150 MPa; P_{back}=1 MPa. Green- KL threshold criterion; Yellow- intensity derivative criterion

4. Spray angle results

The first parameter to be analyzed from the images is the spray opening angle. This value is obtained by producing a linear fit on both the upper and lower spray boundaries within 0.3 mm to 1.5 mm from the nozzle exit and computing the difference in the slope of the two lines so produced.

The spray angle is depicted against the injection pressure in Figure . In this chart, the line color indicates the discharge pressure, while the symbol represents the contour detection method as explained in the previous section. As it could be expected, the clearer trend in the chart is the one corresponding to the discharge pressure variation. As the discharge pressure increases, so does the gas density in the discharge chamber, inducing a higher aerodynamic interaction with the liquid spray. Consequently, the spray tip slows down, and higher air entrainment is promoted. This is consistent with predictions based on the gas-jet analogy, widely used in high-pressure diesel sprays [35]. The injection pressure also produces an increasing trend, thanks to the favorable effect of the injection velocity on the spray atomization and consequently fuel-air mixing. This effect is more evident

for the low discharge pressure condition (1 MPa) and saturates for the higher injection pressures. Considering that the degree of conicity is enough to ensure that no cavitation is taking place, the main reason of this trend is the significance of quiescent air density. When the density is high, its effect on the air entrainment and therefore the mixing process dominates the spray angle trend over turbulence. Instead, when the discharge density is low the mixing process is more affected by the irregularities in the spray boundary induced by the turbulence level. Finally, both criteria provide consistent results in terms of this parameter, showing that macroscopic spray features are not very sensitive to this aspect.

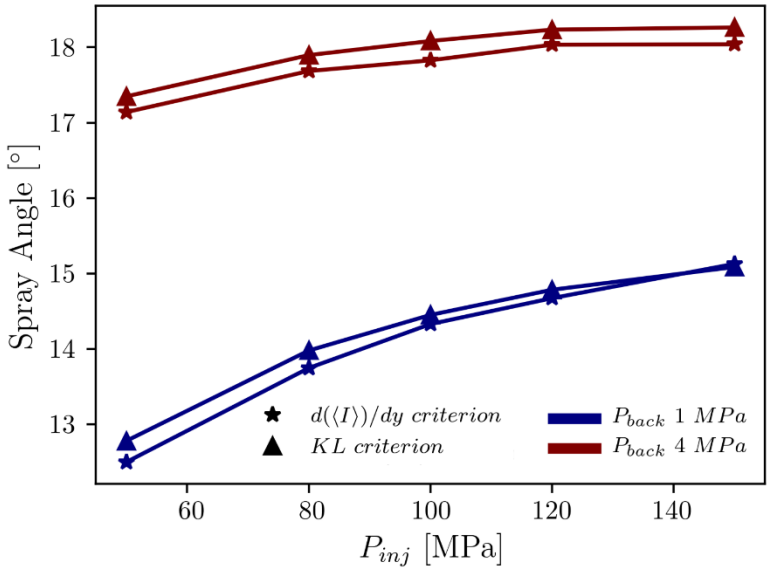

Figure 5: Spray angle as a function of the injection pressure

A further way to quantify the effect of the turbulence level of the flow at the nozzle outlet on the spray morphology can be obtained by looking at the standard deviation of the spray profile itself. The standard deviation is calculated taking the contour detected for each individual image and the one corresponding to an average of all the images corresponding to the quasi-steady region of each injection event. This information is depicted in Figures 6 and 7 for the 1 and 4 MPa discharge pressure conditions, respectively, particularly using the contour detected by the KL threshold criterion.

In the case of the 1 MPa condition, it can be clearly seen how the standard deviation of the spray edge is initially slightly higher for the 50 MPa injection pressure, while very similar for the rest. This behavior is due to the changes in the initial spray structure linked to the primary atomization process. At low injection pressures, the amount of atomized liquid near the nozzle is lower than at higher injection pressure as depicted in Figure 8. This small amount of atomized liquid leads to a less severe light dissipation, which can be appreciated by the lighter color in the upper and lower spray boundary near the injector tip for the 50 MPa case compared to the 150 MPa condition. This difference in the intensity of the light attenuation affects to the repeatability and reliability of the contour detecting methods in this region, which is detected as a higher value in the standard deviation of the contour. However, it has to be mentioned that this situation is seen only very close to the injector tip and does not affect the calculation of other parameters such as the spray angle. Indeed, as the spray develops and primary atomization is almost completed (from approximately 0.7 mm on at any condition) the trend reverses, coming to a situation where the magnitude of this standard deviation is clearly aligned with the injection pressure. This can be seen as a first indication of the turbulence impact on the spray characteristics. Considering the theoretical nozzle outlet velocity computed from Bernoulli's equation, the corresponding Reynolds numbers range 18000 to 32000 depending on the injection pressure, increasing the turbulent intensity and the spray fluctuations. This confirms the suitability of the parameter to act as a marker for the effect of the turbulence intensity on the initial spray development.

Similar situation can be seen in Figure for the 4 MPa discharge pressure case up to an axial position of approximately 1.2 mm. Again, there is a slightly larger standard deviation for the 50 MPa injection pressure, but the enhanced atomization and mixing process induced by the higher discharge pressure helps to significantly reduce the non-

perturbed length (linked to the primary atomization process) and consequently the length needed for this initial deviation to decrease. From that point on, the standard deviation is once more aligned with the level of turbulence induced by the injection pressure. Nevertheless, from 1.2 mm the difference between the injection pressure levels reduces significantly, excluding the lowest condition of 50 MPa. The higher ambient density accelerates secondary atomization processes, driven by the aerodynamic interaction between the initial ligaments and droplets and the ambient gas. This leads to a situation where the oscillations seen in the spray boundary are the result of the spray droplets formed as a result of this secondary atomization, so the effect of the injection conditions is drastically diminished.

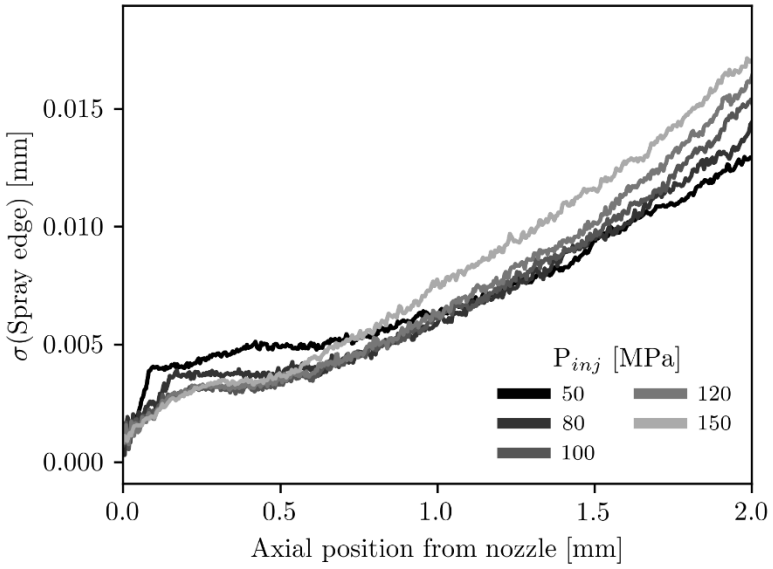

Figure 6: Standard deviation of the spray contour for P_{back}=1 MPa

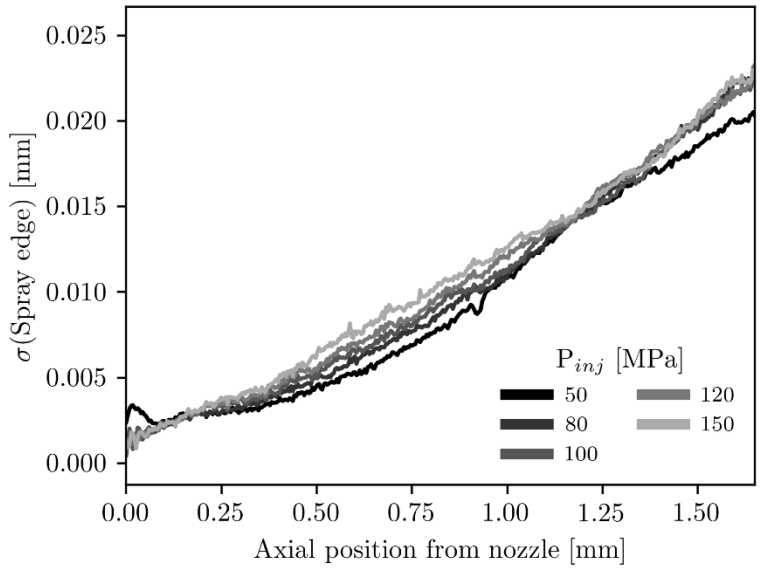

Figure 7: Standard deviation of the spray contour for P_{back}=4 MPa

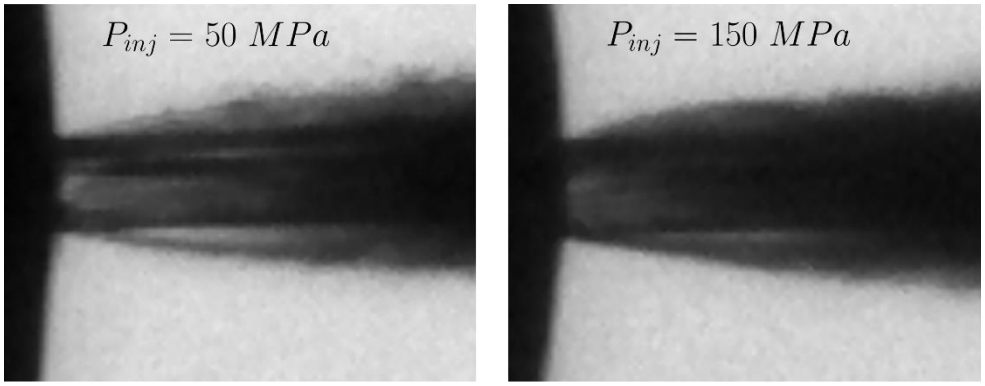

Figure 8: Instantaneous frames of two injection events with P_{back}=1 MPa and P_{inj}=50 MPa (left) and P_{inj}= 150 MPa (right)

Another way to see the variability in the spray features induced by the turbulent flow is seen in Figure 9, which shows the results in terms of the standard deviation of the spray angle. This parameter is computed from a statistical analysis of all the images acquired on each injection event during the quasi-steady operation as well as the 10 test repetitions considered in the study. In this case, only the 1 MPa discharge pressure condition is depicted so that the variation with the injection pressure can be better appreciated. From this figure, it is possible to observe that not only the average spray angle increases with the injection pressure as a consequence of the better atomization and mixing processes, but also the variability of the spray increases. Actually, it can be seen how most of the

variation appears in the range from 50 to 80 MPa, while the increasing trend reduces its slope from that point. This result is similar to what has been previously seen for the nozzle discharge coefficient as a function of the outlet Reynolds number, which shows smaller values in moderate injection pressures as a consequence of a non-fully developed flow regime [36,37]. Again, similar conclusions can be achieved regardless the criterion selected for the contour detection.

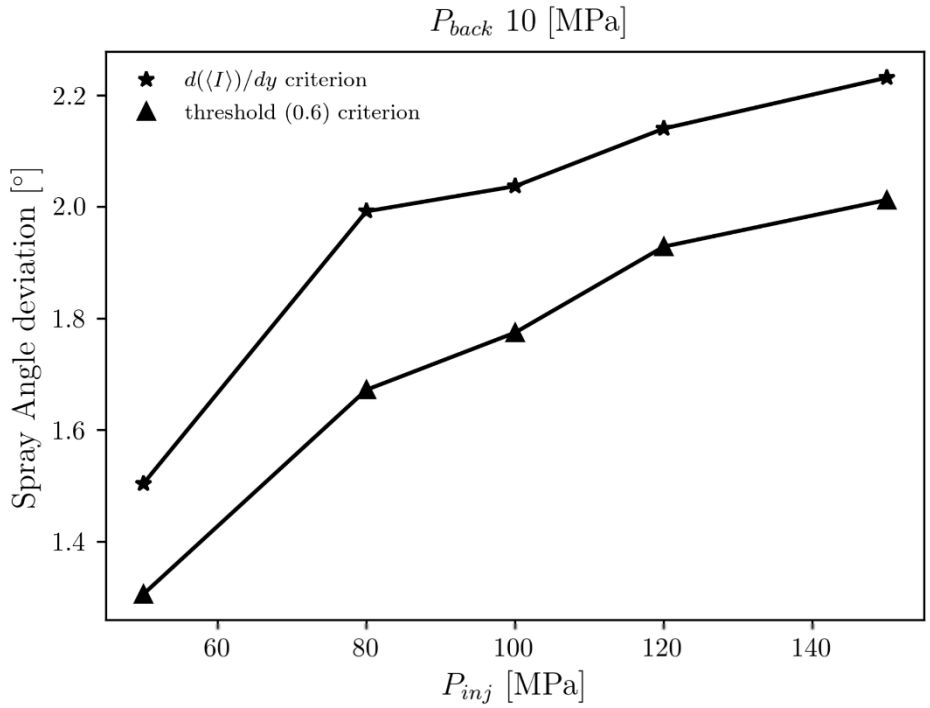

Figure 9: Spray angle standard deviation as a function of the injection pressure

5. Conclusions

In the current paper, an investigation of the effect of the injection conditions on the near-nozzle spray development is performed. For this purpose, a high speed and high magnification DBI technique is performed on a constant-volume chamber filled with pressurized nitrogen. The work is mainly focused on the influence of the injection pressure (and therefore spray outlet velocity), with values ranging 50 to 150 MPa.

However, a sensitivity on the discharge pressure is also analyzed, with values of 1 and 4 MPa.

The spray images obtained using this methodology are processed using two different criteria to detect the spray boundary: one using a threshold on KL, and a second one based on the intensity derivative. From both profiles, several parameters including the average spray angle, the standard deviation of this angle and the standard deviation of the spray boundary itself (taking as a reference an average image) are computed and analyzed vs. the injection pressure. The following conclusions were drawn:

- Macroscopic spray features are mostly insensitive to the criterion used for the spray contour detection. However, it can be seen how the pressure derivative provides slightly higher variability in the spray boundary compared to the KL threshold processing.
- The spray angle in the near-field region is mostly a function of the discharge pressure, linked to the effect of the ambient density on the atomization and fuel-air mixing processes. However, a non-negligible effect of the fuel injection pressure is also observed, especially at low ambient density.
- The standard deviation of the spray angle in this same region also increases with the injection pressure. This is related to the turbulence intensity, which also increases with this pressure due to the higher outlet velocities achieved. This effect is more significant when moving from 50 to 80 MPa, while the variation is smaller in the rest of the range.
- After an short initial region linked to the primary atomization process, the standard deviation computed inside the spray contour is mostly related to the fuel injection pressure, also as a consequence of the turbulence impact. This effect is more significantly appreciated in the 1 MPa discharge pressure condition, where

aerodynamic interactions between the spray and the discharge gas are less significant, and therefore turbulence-induced oscillations are more relevant.

ACKNOWLEDGEMENTS

This research has been funded by the Spanish Ministerio Ciencia e Innovación through the project RTI2018-099706-B-100: “Estudio de la atomización primaria mediante simulaciones DNS y técnicas ópticas de muy alta resolución”. González-Montero L.A. is partially supported though the contract FPI – Subprograma 2 of the Universitat Politècnica de València.

REFERENCES

[1] Oh H, Bae C. Effects of the injection timing on spray and combustion characteristics in a spray-guided DISI engine under lean-stratified operation. Fuel 2013;107:225–35. doi:10.1016/j.fuel.2013.01.019.

[2] Roque A, Foucher F, Lamiel Q, Imoehl B, Lamarque N, Helie J. Impact of gasoline direct injection fuel films on exhaust soot production in a model experiment. Int J Engine Res 2020;21:367–90. doi:10.1177/1468087419879851.

[3] Payri R, Salvador FJ, Manin J, Viera A. Diesel ignition delay and lift-off length through different methodologies using a multi-hole injector. Appl Energy 2016;162:541–50. doi:10.1016/j.apenergy.2015.10.118.

[4] Chartier C, Aronsson U, Andersson Ö, Egnell R, Johansson B. Influence of jet-jet interactions on the lift-off length in an optical heavy-duty DI diesel engine. Fuel 2013;112:311–8. doi:10.1016/j.fuel.2013.05.021.

[5] Xuan T, Pastor J V., García-Oliver JM, García A, He Z, Wang Q, et al. In-flame soot quantification of diesel sprays under sooting/non-sooting critical conditions in an optical engine.

Appl Therm Eng 2019;149:1–10. doi:10.1016/j.applthermaleng.2018.11.112.

[6] Jakob M, Hülser T, Janssen A, Adomeit P, Pischinger S, Grünefeld G. Simultaneous high-speed visualization of soot luminosity and OH * chemiluminescence of alternative-fuel combustion in a HSDI diesel engine under realistic operating conditions. Combust Flame 2012;159:2516–29. doi:10.1016/j.combustflame.2012.03.004.

[7] Pickett LM. Low flame temperature limits for mixing-controlled Diesel combustion. Proc Combust Inst 2005;30:2727–35. doi:10.1016/j.proci.2004.08.187.

[8] Chen B, Feng L, Wang Y, Ma T, Liu H, Geng C, et al. Spray and flame characteristics of wall-impinging diesel fuel spray at different wall temperatures and ambient pressures in a constant volume combustion vessel. Fuel 2019;235:416–25. doi:10.1016/j.fuel.2018.07.154.

[9] Maes N, Hooglugt M, Dam N, Somers B, Hardy G. On the influence of wall distance and geometry for high-pressure n-dodecane spray flames in a constant-volume chamber. Int J Engine Res 2019. doi:10.1177/1468087419875242.

[10] Yamasaki Y, Ikemura R, Takahashi M, Shimizu F, Kaneko S. Simple combustion model for a diesel engine with multiple fuel injections. Int J Engine Res 2019;20:167–80. doi:10.1177/1468087417742764.

[11] Huang H, Zhu Z, Chen Y, Chen Y, Lv D, Zhu J, et al. Experimental and numerical study of multiple injection effects on combustion and emission characteristics of natural gas–diesel dual-fuel engine. Energy Convers Manag 2019;183:84–96. doi:10.1016/j.enconman.2018.12.110.

[12] Payri R, De La Morena J, Monsalve-Serrano J, Pesce FC, Vassallo A. Impact of counter-bore nozzle on the combustion process and exhaust emissions for light-duty diesel engine application. Int J Engine Res 2019;20:46–57. doi:10.1177/1468087418819250.

[13] Liu W, Song C. Effect of post injection strategy on regulated exhaust emissions and particulate matter in a HSDI diesel engine. Fuel 2016;185:1–9. doi:10.1016/j.fuel.2016.07.057.

[14] Park H, Bae C, Ha C. A comprehensive analysis of multiple injection strategies for improving

diesel combustion process under cold-start conditions. Fuel 2019;255:115762. doi:10.1016/j.fuel.2019.115762.

[15] Dumouchel C. On the experimental investigation on primary atomization of liquid streams. Exp Fluids 2008;45:371–422. doi:10.1007/s00348-008-0526-0.

[16] Zhao L, Wang M, Wang P, Zhu X, Qiu Q, Shen S. Experimental study on the internal flow field and spray characteristics of hollow nozzle. Appl Therm Eng 2018;144:757–68. doi:10.1016/j.applthermaleng.2018.06.047.

[17] Battistoni M, Som S, Powell CF. Highly resolved Eulerian simulations of fuel spray transients in single and multi-hole injectors: Nozzle flow and near-exit dynamics. Fuel 2019;251:709–29. doi:10.1016/j.fuel.2019.04.076.

[18] Desantes JM, Payri R, Salvador FJ, De la Morena J. Influence of cavitation phenomenon on primary break-up and spray behavior at stationary conditions. Fuel 2010;89:3033–41. doi:10.1016/j.fuel.2010.06.004.

[19] Abderrezzak B, Huang Y. A contribution to the understanding of cavitation effects on droplet formation through a quantitative observation on breakup of liquid jet. Int J Hydrogen Energy 2016;41:15821–8. doi:10.1016/j.ijhydene.2016.04.209.

[20] Zandian A, Sirignano WA, Hussain F. Planar liquid jet: Early deformation and atomization cascades. Phys Fluids 2017;29. doi:10.1063/1.4986790.

[21] Shinjo J, Umemura A. Surface instability and primary atomization characteristics of straight liquid jet sprays. Int J Multiph Flow 2011;37:1294–304. doi:10.1016/j.ijmultiphaseflow.2011.08.002.

[22] Reitz RD, Beale JC. Modeling Spray Atomization With the Kelvin-Helmholtz/Rayleigh-Taylor Hybrid Model. At Sprays 2014;9:623–50. doi:10.1615/atomizspr.v9.i6.40.

[23] Wetzel J, Henn M, Gotthardt M, Rottengruber H. Experimental Investigation of the Primary Spray Development of GDI Injectors for Different Nozzle Geometries 2015. doi:10.4271/2015-

01-0911.Copyright.

[24] Magnotti GM, Genzale CL. Exploration of Turbulent Atomization Mechanisms for Diesel Spray Simulations. SAE Tech Pap 2017. doi:10.4271/2017-01-0829.

[25] Jiao D, Zhang F, Du Q, Niu Z, Jiao K. Direct numerical simulation of near nozzle diesel jet evolution with full temporal-spatial turbulence inlet profile. Fuel 2017;207:22–32. doi:10.1016/j.fuel.2017.06.032.

[26] Kim B, Park S. Effect of orifice inlet roundness on internal flow and external spray characteristics in enlarged nozzle with single-passage. Exp Therm Fluid Sci 2019;109:109875. doi:10.1016/j.expthermflusci.2019.109875.

[27] Linne M, Paciaroni ME, Hall T, Parker T. Ballistic imaging of the near field in a diesel spray. Exp Fluids 2006;40:836–46. doi:10.1007/s00348-006-0122-0.

[28] Payri R, Salvador FJ, Gimeno J, De la Morena J. Analysis of Diesel spray atomization by means of a near-nozzle field visualization technique. At Sprays 2011;21:753–74. doi:10.1615/AtomizSpr.2012004051.

[29] Duke DJ, Kastengren AL, Matusik KE, Swantek AB, Powell CF, Payri R, et al. Internal and near nozzle measurements of Engine Combustion Network “Spray G” gasoline direct injectors. Exp Therm Fluid Sci 2017;88:608–21. doi:10.1016/j.expthermflusci.2017.07.015.

[30] Payri R, Bracho G, Marti-Aldaravi P, Viera A. Near field visualization of diesel spray for different nozzle inclination angles in non-vaporizing conditions. At Sprays 2017;27:251–67. doi:10.1615/AtomizSpr.2017017949.

[31] Manin J, Bardi M, Pickett LM, Dahms RN, Oefelein JC. Microscopic investigation of the atomization and mixing processes of diesel sprays injected into high pressure and temperature environments. Fuel 2014;134:531–43. doi:10.1016/j.fuel.2014.05.060.

[32] Salvador FJ, Carreres M, De la Morena J, Martínez-Miracle E. Computational assessment of temperature variations through calibrated orifices subjected to high pressure drops: Application

to diesel injection nozzles. Energy Convers Manag 2018;171:438–51. doi:10.1016/j.enconman.2018.05.102.

[33] Caudwell DR, Trusler JPM, Vesovic V, Wakeham WA. The viscosity and density of n-dodecane and n-octadecane at pressures up to 200 MPa and temperatures up to 473 K. Int J Thermophys 2004;25:1339–52. doi:10.1007/s10765-004-5742-0.

[34] Payri R, Gimeno J, Cardona S, Ayyapureddi S. Experimental study of the influence of the fuel and boundary conditions over the soot formation in multi-hole diesel injectors using high-speed color diffused back-illumination technique. Appl Therm Eng 2019;158:113746. doi:10.1016/J.APPLTHERMALENG.2019.113746.

[35] Spalding DB. Combustion and mass transfer. Pergamon Press; 1979.

[36] Desantes JM, Lopez JJ, Carreres M, López-Pintor D. Characterization and prediction of the discharge coefficient of non-cavitating diesel injection nozzles. Fuel 2016;184:371–81. doi:10.1016/j.fuel.2016.07.026.

[37] Lichtarowicz AK, Duggins RK, Markland E. Discharge coefficients for incompressible non-cavitating flow through long orifices. J Mech Engng Sci 1965;7:210–9.